Geomorphology 122 (2010) 153–166

Contents lists available at ScienceDirect

Geomorphology

journal homepage: www.elsevier.com/locate/geomorph

Combining spatial data in landslide reactivation susceptibility mapping: A likelihood ratio-based approach in W Belgium

Olivier Dewitte [a,b,*], Chang-Jo Chung [c], Yves Cornet [d], Mohamed Daoudi [b], Alain Demoulin [b,e]

[a] Land Management and Natural Hazards Unit, Institute of Environment and Sustainability, DG Joint Research Centre, European Commission, Italy
[b] Unit of Physical Geography and Quaternary, Department of Geography, University of Liège, Belgium
[c] University of Ottawa, Department of Earth Sciences, University of Ottawa, Canada
[d] Unit of Geomatics, Department of Geography, University of Liège, Belgium
[e] Belgian National Fund for Scientific Research, Belgium

ARTICLE INFO

Article history:
Received 29 January 2010
Received in revised form 25 May 2010
Accepted 3 June 2010
Available online 19 June 2010

Keywords:
Landslide susceptibility mapping
Spatial data combination
Cross-validation
Expert knowledge
Landslide reactivation
Belgium

ABSTRACT

A key issue in landslide susceptibility mapping concerns the relevance of the spatial data combination used in the prediction. Various combinations of high-resolution predictor variables and possibilities of selecting them from a larger dataset are analysed. The scarp reactivation of several landslides in a hilly region of W Belgium is investigated at the pixel scale. The susceptibility modelling uses the reactivated scarp segments as the dependent variable and 13 factors at a 2 m-resolution related to topography, hydrology, land use and lithology as potential independent variables. The modelling uses a likelihood ratio approach based on the comparison, for each independent variable, between two empirical distribution functions (EDFs), respectively for the reactivated and non-reactivated areas. It uses these EDFs as favourability values to build membership values and combine them with a fuzzy Gamma operator. Five different data combinations are tested and compared by analysing the prediction-rate curves obtained by cross-validation. The geomorphological value of the resulting susceptibility maps is also discussed. This research shows relevant results for predicting the susceptibility to scarp reactivation. We highlight the need for testing several data combinations and underline that combining quantitative criteria with expert opinion is an asset for reliable predictions.

1. Introduction

Landslide prediction has concerned many studies over the last decade (Dai et al., 2002; Glade and Crozier, 2005; Van Westen et al., 2006; Van Asch et al., 2007; Fell et al., 2008). It involves the concepts of susceptibility, i.e. the spatial distribution of landslides which exist or potentially may occur in an area, and hazard, which includes the probability of landslide occurrence within a given period of time. At first, a landslide prediction focuses on the susceptibility evaluation which has to be considered independently of the temporal issue. The spatial aspect is related to a particular combination of predisposing environmental factors (or predictor variables), whereas the latter one depends on the probability of occurrence of time-dependent triggering factors such as earthquakes and heavy rainfall.

The methods for predicting landslide susceptibility range from purely qualitative evaluations to complex quantitative models, and rely all on the basic assumption that landsliding is controlled by variables that can be determined empirically, statistically or by process-based experiment (Glade and Crozier, 2005; Van Asch et al., 2007). The statistical methods such as GIS-based bivariate, multivariate, and probabilistic analyses are capable of predicting the spatial distribution of landslides with a relatively small amount of data (Glade and Crozier, 2005; Van Westen et al., 2006; Van Asch et al., 2007), the spatial information on landslide initiation locations being used in combination with several environmental factors. They can also give reliable results at scales adequate for the design of hazard mitigation and land development (>1:10,000) (e.g., Thiery et al., 2007).

Comparing several statistical techniques for predicting landslide susceptibility is frequent (e.g. Pistocchi et al., 2002; Brenning, 2005; Lee and Pradhan, 2007; Lee et al., 2007; Akgun et al., 2008; Ercanoglu et al., 2008; Nefeslioglu et al., 2008; Van Den Eeckhaut et al., 2009; Yilmaz, 2009; Rossi et al., 2010) and it often reveals, independently of the combination of environmental factors, marginal differences between the prediction results. On the other hand, a key issue concerns the selection of the factors to be inserted in the combination (e.g. Pistocchi et al., 2002; Van Westen et al., 2003; Regmi et al., 2010). Unfortunately, due to the lack of information or to some limitations of the data set, in particular the inappropriate resolution of the Digital

* Corresponding author. Land Management and Natural Hazards Unit, Institute of Environment and Sustainability, DG Joint Research Centre, European Commission, Italy. Tel.: +39 0332 78 9316; fax: +39 0332 78 6394.
E-mail address: olivier.dewitte@jrc.ec.europa.eu (O. Dewitte).

0169-555X/$ – see front matter © 2010 Elsevier B.V. All rights reserved.
doi:10.1016/j.geomorph.2010.06.010

Terrain Model (DTM), potentially contributing factors have frequently to be omitted in a prediction (Van Westen et al., 2008), which restricts some combinations of variables to be tested.

The main scope of this research is to analyse the relevance of various high-resolution spatial data combinations in landslide susceptibility mapping and discuss possibilities of selecting them from a larger dataset. To this end, we apply a probabilistic model to the reactivation of large landslides in West Belgium using high-resolution DTMs. Van Den Eeckhaut et al. (2006, 2009) have already mapped susceptibility to landsliding in this area applying several statistical approaches based on topographical units and grid cells. Whereas their research concerned the occurrence of new landslides, our study is focussing at the pixel scale on the prediction of landslide reactivation that represents by far the highest hazard related to slope instability in this area (Van den Eeckhaut, 2006). More precisely, the study area corresponds to landslide main scarps and the resulting susceptibility maps locate the parts of pre-existing landslide scarps most prone to reactivation. A particular focus will be on the significance of the predictor variables as well as the validation of the predictions. The role of the geomorphologist's expertise in the modelling procedure will be pointed up not only in the input data extraction and selection, but also in the evaluation of the mathematically obtained landslide susceptibility maps.

2. Study area

More than 150 large landslides are scattered over the loose tertiary sediment cover forming the hilly area of the Flemish Ardennes in west Belgium (Van Den Eeckhaut et al., 2005) (Fig. 1A). These landslides are classified as deep-seated and are rotational and complex earth slides. No new landslide has developed for decades and due to the absence of written document describing a landslide initiation they are all assumed to predate 1900 AD (Van Den Eeckhaut, 2006). They might have been initiated under periglacial conditions, possibly in response to a seismic trigger associated with a period of intense rainfall (Van Den Eeckhaut, 2006; Van Den Eeckhaut et al., 2007a). According to Keefer's (1984) relation between maximum distance of landslides from a fault and Richter magnitude ML, magnitudes between 5 and 6 were estimated necessary to trigger landslides in the Flemish Ardennes (Van Den Eeckhaut, 2006). However, no landslide was reported despite the magnitude ML 5.6 earthquake of June 1938 in the Flemish Ardennes, this event being the biggest earthquake recorded in Belgium during the 20th century. Actually, the hazard associated with slope movements in this area corresponds to ground movements within these pre-existing landslides. Two kinds of slope processes, corresponding to either reactivations at a deeper level or shallower motions are distinguished (Dewitte et al., 2009). The former re-use pre-existing surfaces of rupture located at depths of ~15–20 m and are associated with the largest movements. They are also smaller reactivations confined at the landslide head. The other displacements consist in (1) earth flows occurring in the zone of accumulation sometimes as a consequence of large upslope reactivations, and (2) small failures occurring randomly. The higher hazard is related to the reactivations. Interviews and analysis of written documents stressed that ~15% of the landslides were affected by reactivation over the last two decades (Van Den Eeckhaut, 2006), which is a minimum value with regard to the decadal-scale analysis of ground movements of several representative landslides performed by Dewitte et al. (2009) with multi-temporal DTM comparisons. While most reactivations were triggered by intense rainfall, their spatial and temporal distributions are strongly related to the nature of the vegetation cover and the human activity (Van Den Eeckhaut et al., 2007b; Dewitte et al., 2008, 2009). The region has a maritime temperate climate with an average temperature of ~10 °C and a mean annual rainfall of 800 mm which is well-distributed over all the season.

As a compromise between high resolution and reasonable processing time, we focussed on the reactivation of 13 representative landslides. They extend on two hills which culminate at altitudes between 75 and 85 masl and are situated along the river Scheldt close to the town of Oudenaarde (Fig. 1B). Three landslides extend on the Leupegem hill, to the north, and 10 are developed on the Rotelenberg hill, to the south (Fig. 1B). The landslides are carved in an alternation of Eocene subhorizontal clayey sand and clay layers on which a perched water table can expand (Jacobs et al., 1999). They are all in contact with the Aalbeke Member of the Kortrijk Formation, which consists of 10-m-thick homogeneous blue massive clays and is recognized as the layer most sensitive to landsliding (Fig. 1B). They have a mean size of ~6 ha (from 2 to 10 ha), a length of ~320 m, and a width of ~175 m, and their ~8-m-high main scarp delimits the abrupt fringe of the plateaus (Dewitte and Demoulin, 2005). They developed on slopes of 13–20%, preferentially oriented to the W and N. Through morphometric measurements, the mean depth of the surface of rupture has been estimated in the range 15–20 m, implying a mean displaced volume of ~300 000 m^3 (Dewitte and Demoulin, 2005; Dewitte et al., 2008, 2009). The landslides are mainly covered by pastures and forests (mainly beech and poplar trees), while their main scarps are almost completely forested (except for landslides 3, 4, and 10). Forest dominates within landslides 7, 8, 9, 11, 12 and 13 while pasture extends almost exclusively at the foot of landslides 9 and 10 (Dewitte, 2006). Cultivated land predominates upslope of the landslide crowns, with limited change over time, and a very small area is covered by buildings. The land use percentages remained similar during the 1952–1996 period (Dewitte et al., 2009).

3. Spatial data used in the modelling

The first step in our data collection was to define the extent of the 13 main scarps, i.e. the study area, and to localise their reactivated sections. To do this, we used multi-temporal DTMs of the Leupegem and Rotelenberg hills (Fig. 1B) for two periods (1952 and 1996). From ground points and scarp lines extracted by aerial digital stereophotogrammetry, the DTM grids were generated at a 2 m-resolution with a final accuracy ranging between ~45 and 65 cm (Dewitte et al., 2008). The lines of pixels derived from the top lines of the main scarps used for the DTM generation are not considered as such for the study area. Due to data alteration during the vector–raster conversion, most of those pixels are extending only partly on the real scarp. Actually, the study area concerns all the pixels downslope of the top of the scarps and totally located on the visible part of the surface of rupture, which corresponds fairly well to the real scarp area (Dewitte, 2006). In total, the study area covers 6293 pixels at the 2 m-resolution, which represents by far enough data to construct robust statistical models (Demoulin and Chung, 2007; Hjort and Marmion, 2008). From the comparison of these DTMs for the two epochs, 14 areas of scarp retreat >2 m corresponding to reactivation (Fig. 2A) were identified within the 13 main scarps (Dewitte et al., 2009). This 2 m threshold value corresponds to the 95% confidence level derived from the RMS error of the DTMs. In total, 1268 pixels are in the reactivated sections, which means that ~20% of the study area was affected by these slope movements during the 1952–1996 period.

The potential predisposing factors used as independent variables in the modelling were extracted from the DTMs of 1952 and 1996, the land use maps derived from the orthophotos obtained with the aerial photographs used in the DTM extraction, and the 1:50 000 digital lithological map updated in 2001 by the Flemish Government. All the variables are extracted at the 2-m pixel size. Working at the resolution of the DTMs allowed us to generate all the potential predisposing factors that we consider relevant for the assessment of landslide reactivation process. The lithological map is however not that precise and, for this reason, the uncertainty related to its boundaries will be considered in the modelling (See Section 5.2). The 13 potential predictor variables are presented in Table 1.

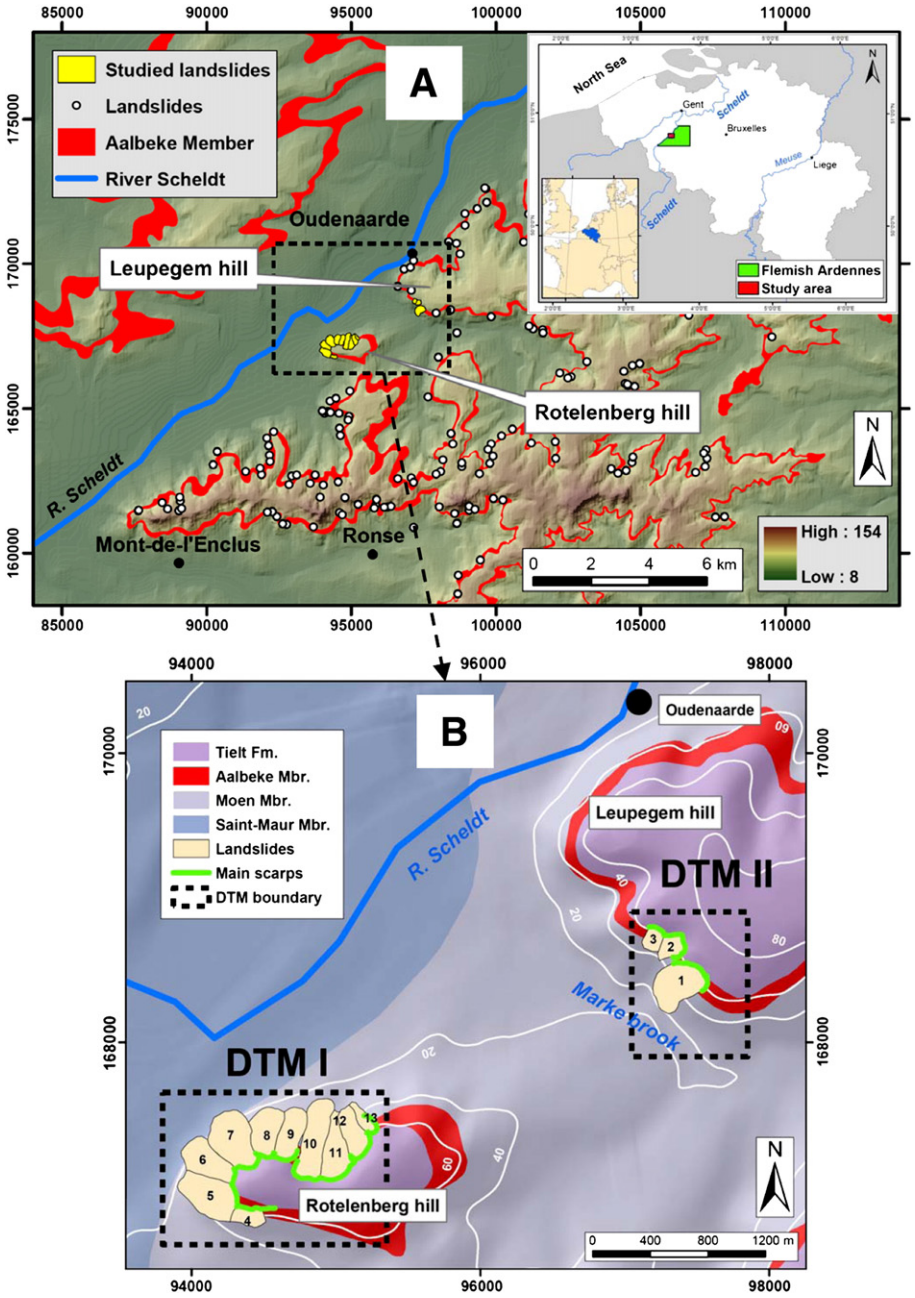

Fig. 1. Location map of the study area. (A) General view of the Flemish Ardennes. The LIDAR-derived topography and the shaded map are from the DEM of Flanders acquired in 2002 and published in 2005 by OC GIS-Vlaanderen [MVG,-LIN-AWZ and MVG-LIN-ANIMAL]). The landslides in yellow correspond to the mass movements whose main scarps are investigated in this research. The white circles locate the other landslides that have been located in the Flemish Ardennes by Van Den Eeckhaut (2006). (B) Lithological setting of the two investigated hills. The scars and the main scarps of the landslides are superposed on the Eocene lithologies. The main scarps represent the area investigated for the modelling. The quadrangles DTM I and DTM II locate the DTMs used in the modelling. The altitudes (in white) and coordinates (Belgian Lambert 72) are in meters.

The predictor variables were all computed with the 1952 and 1996 data (with ArcGIS 9.0 dedicated functions), except for the lithology. Since the reactivated parts (Fig. 2) correspond to slope movements that have occurred between 1952 and 1996, the 1952 predictor variables allowed us to consider the pre-failure conditions, i.e. those that led to slope reactivation and are not the consequence of it (Atkinson and Massari, 1998; Van Den Eeckhaut et al., 2006; Nefeslioglu et al., 2008). In the same way, the 1996 data will be used for computing the post-1996 probabilities.

Three morphological data were directly computed from the DTMs: elevation, slope angle and slope aspect. Elevation was not considered here as a factor reflecting rainfall repartition, the two hills being very close and having a similar relief. It was actually chosen as a proxy indicator of the groundwater conditions. The lithology has a subhorizontal structure; the higher on a hillslope a pixel is located, the more chances the groundwater level has to be deep.

The high resolution of the DTMs permitted a particular focus on the surface runoff. Several variables were considered as relevant. They define locations of water concentration and therefore represent potential places where slope instability can increase after rainfall events:

- flow accumulation which represents the number of cells that flows into each downslope cell, or in other words, is a measure of the land area that contributes runoff to the pixel;

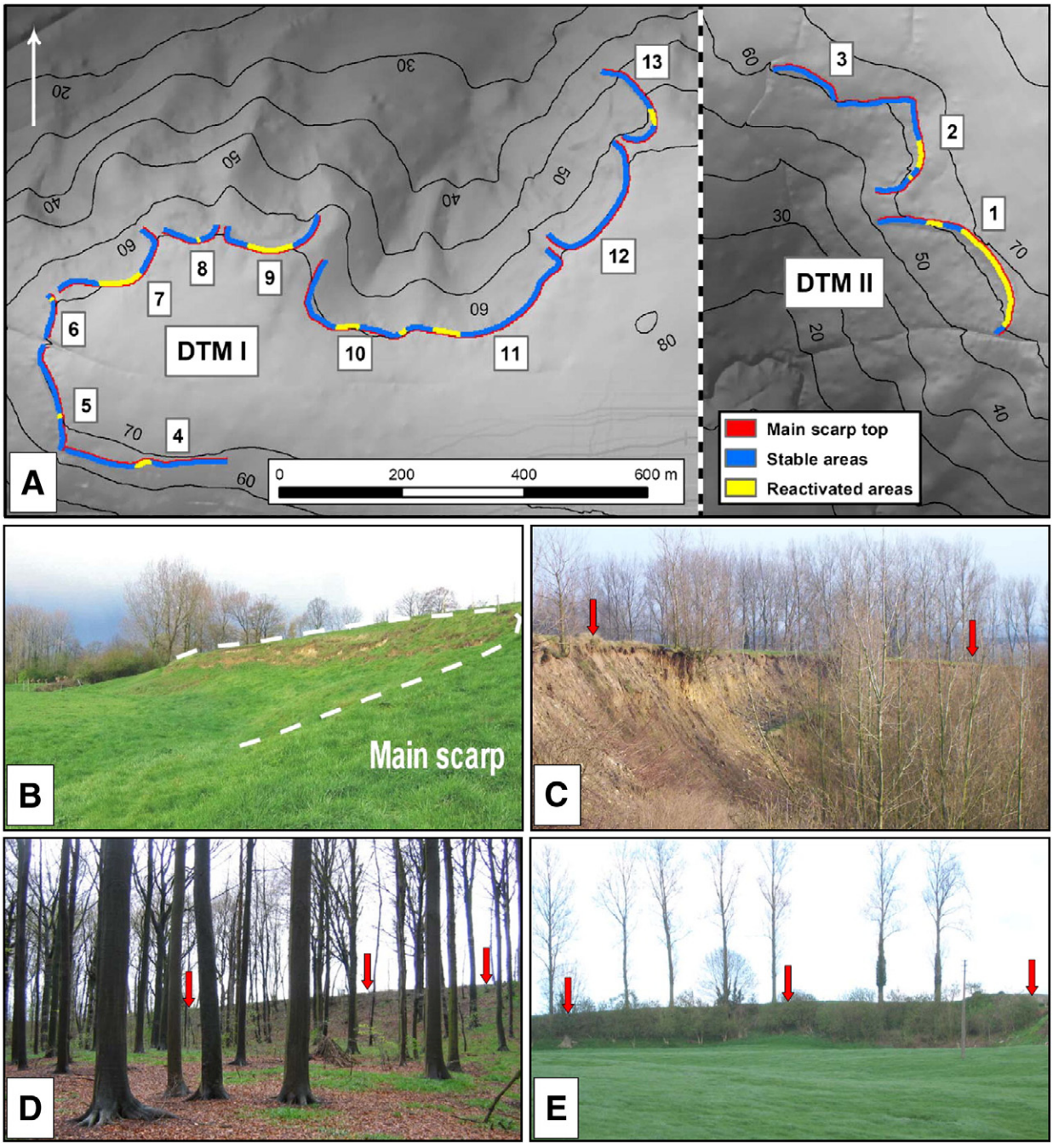

Fig. 2. Study area and landslide scarps studied. (A) Fourteen occurrences of scarp retreat (reactivated areas) measured between 1952 and 1996 from the comparison of two 2-m DTMs extracted by aerial digital stereophotogrammetry. The 1952 setting (shown here) corresponds to the pre-reactivation conditions. (B) Reactivation of a scarp in pasture: view towards the W of the pre-1996 reactivated main scarp of landslide 4 (April 2004). The lateral extension of the main scarp is ~60 m. The white dashed line marks the scarp. (C) Reactivation of a forested scarp: view towards the SE of the February 1995 reactivated main scarp of landslide 1 (February 2003). (D) Stable scarp under forest: view towards the SE of the landslide 8 main scarp (April 2004). (E) Stable scarp in pasture: view towards the E of the landslide 3 main scarp (April 2004).

- focal flow which corresponds to local flow concentration involving the surrounding eight pixels. Its resulting values measure flow into, and not out of a cell;
- profile and planform curvatures which control the flow of water in and out of the slopes. These variables were computed with the surrounding eight pixels; and
- distance from stream network which is the Euclidean distance from the stream channel network simulated based on flow accumulation data. Each pixel with a flow accumulation value exceeding 2000 pixels was classified as a stream. The use of this threshold value resulted in a drainage area of 8 ha as the one observed for incipient gully development in Central Belgium (Poesen et al., 2003).

Two geological data layers were extracted from the digital lithological map. The variable "lithology" includes four rock types (from the most recent to the oldest): Tielt Formation (clayey sand alternating with clay layers), Aalbeke Member (clay), Moen Member (clayey coarse silt to fine sand with clay layers), and Saint-Maur Member (silty clay). The "distance from Aalbeke Member" is the Euclidean distance from the Aalbeke clays, the most sensitive to landsliding.

The role of vegetation was taken into account through three predictor variables. Four different classes were distinguished in the "Land use" layer: cultivation, meadow, forest and built area (roads and houses). "Distance from cultivation" which corresponds to the

Table 1
Description of the 13 potential predictor variables used in the modelling.

Variable	Unit	Type*	Original data**
Elevation	m	1	DTMs
Slope angle	Degrees	1	DTMs
Slope aspect	Degrees	1	DTMs
Flow accumulation	Pixels	1	DTMs
Focal flow	Pixels	1	DTMs
Profile curvature	1/100 m	1	DTMs
Planform curvature	1/100 m	1	DTMs
Distance from stream network	m	1	DTMs
Land use	Class	2	Orthophotos
Lithology	Class	2	Rock type map
Distance from cultivation	m	1	Orthophotos
Distance from Aalbeke Member	m	1	Lithological map
Vegetation index	Pixel m^{-1}	1	Orthophotos, DTMs

*Type 1 means continuous variable and type 2 means categorical variable.
**Both DTMs and orthophotos of 1952 and 1996 were used to derive the variables.

Euclidean distance from the nearest cultivation located upstream of the main scarps was constructed to consider the important role that cultivation can have on surface runoff, especially during the winter when bare soils can represent a large part of the cultivated areas. In order to approximate the interplay between the concentration of the surface runoff within the cultivation and its infiltration along its flow, the "vegetation index" was computed. It corresponds to the flow accumulation through the cultivated areas located upstream of the main scarp and weighted by the length of the flow.

The errors related to the DTMs can have an impact on the reliability of the variables. This impact is quite difficult to quantify, but it can be more or less important according to the type of variable considered. For the "elevation" it is negligible since it concerns an error of a few tens of centimetres over several tens of meters. On the other hand, the impact on the variables derived from the DTMs can be more significant, especially where the topographic surface is quite flat (Chang and Tsai, 1991; Florinsky, 1998). Since the study area concerns the main scarps of the landslides, where the slope angles are large (>15%; Dewitte, 2006), the impact of the errors should be very limited on the variables where the computation relies only on the topographical characteristics of the scarps: slope angle, slope aspect, focal flow, and profile and planform curvatures. However, flow accumulation should be more sensitive since it depends mainly on the topographic configuration in the flatter areas upslope of the main scarps. A small elevation error can modify the direction of the flow and hence its accumulation. If it happens in the upslope part of the watershed, close to the drainage divide where the accumulation values are small, such a modification should be very limited. On the other hand, downslope, the accumulations are larger and a modification in the direction can give a pixel a value far from the reality. Along the main scarp lines, the lateral variability of flow accumulation can be very important from one pixel to the other (Dewitte, 2006). Since the DTM errors are randomly distributed (Dewitte et al., 2008), no trend should appear in the accumulation errors; therefore, the errors along the scarps should concern in each time very small groups of pixels randomly spread out and independent from each other. Actually, the impact of the errors on the real pattern of flow accumulation is very limited, as it is attested by field observations (Dewitte, 2006).

4. Methodology

4.1. Quantitative model

Several favourability function models have been developed for predicting landslide susceptibility (Chung and Fabbri, 2005; Chung, 2006; Demoulin and Chung, 2007). The model used here is an adaptation of the fuzzy set membership function proposed by Chung and Fabbri (2008) in combination with the fuzzy set operator approach developed by Chung and Fabbri (2001). The model is based on the likelihood ratio function of multivariate frequency distributions calculated for predictor variables (Chung, 2006). Beyond easy calculation, the advantage of this probabilistic approach lies in yielding significant results already with small datasets. It allows us to work at the pixel scale and analyze continuous and categorical data layers simultaneously without converting one type of data into another. This hybrid approach also allows the introduction of the expert knowledge in the factor selection.

Consider a study area with m spatial data layers (predictor variables). To predict landslide reactivation the area is divided into two non-overlapping sub-areas, the "reactivated" (denoted by **M**) and "stable" (denoted by $\overline{\mathbf{M}}$) ones (Fig. 2). To provide useful information for identifying reactivation locations, the predictor variables in reactivated areas should have ranges of values that differ significantly from those in stable terrains. Thus the frequency distributions of variables for both areas should also be distinctly different. The likelihood ratio function is the ratio of the two frequency distributions and highlights the difference between the two areas. Consider a pixel p with m pixel values $(p_1,\cdots,p_m)$ in a study area, one for each data layer. Let $\boldsymbol{f}\{p_1,\cdots, p_m|\mathbf{M}\}$ and $\boldsymbol{f}\{p_1,\cdots,p_m|\overline{\mathbf{M}}\}$ be the multivariate frequency distribution functions assuming that a pixel is from **M**, and from $\overline{\mathbf{M}}$, respectively.

Then, the multivariate likelihood ratio function that the pixel p will belong to a future reactivation is defined as:

$$\lambda(p: p_1,\cdots,p_m) = \frac{\boldsymbol{f}\{p_1,\cdots,p_m|\,\mathbf{M}\}}{\boldsymbol{f}\{p_1,\cdots,p_m|\,\overline{\mathbf{M}}\}} \quad (1)$$

Consider a pixel p in the study area with values $(x_1,\cdots, x_k, y_1,\cdots, y_h)$; the first k values $(x_1,\cdots, x_k)$ correspond to categorical variables and the remaining h values $(y_1,\cdots, y_h)$ represent continuous variables and m = k + h. Let $\boldsymbol{f}\{x_1,\cdots, x_k, y_1,\cdots, y_h|\mathbf{M}\}$ and $\boldsymbol{f}\{x_1,\cdots, x_k, y_1,\cdots, y_h|\overline{\mathbf{M}}\}$ be the multivariate frequency distribution functions assuming that a pixel is from **M**, and from $\overline{\mathbf{M}}$, respectively. Then the multivariate likelihood ratio function in Eq. (1) is denoted by:

$$\lambda(p: x_1,\cdots,x_k,y_1,\cdots,y_h) = \frac{\boldsymbol{f}\{x_1,\cdots,x_k,y_1,\cdots,y_h|\mathbf{M}\}}{\boldsymbol{f}\{x_1,\cdots,x_k,y_1,\cdots,y_h|\overline{\mathbf{M}}\}} \quad (2)$$

To estimate $\lambda(p{:}x_1,\cdots, x_k, y_1,\cdots, y_h)$, the m categorical and continuous predictor variables are assumed to be statistically independent and hence:

$$\lambda(p: x_1,\cdots,x_k,y_1,\cdots,y_h) = \lambda(p: x_1,\cdots,x_k)\cdot\lambda(p: y_1,\cdots,y_h) \quad (3)$$

The likelihood ratio function of Eq. (3) is estimated as a multiple of two estimated likelihood ratio functions: $\lambda(p{:}x_1,\cdots, x_k)$ for the categorical data layers and $\lambda(p{:}y_1,\cdots, y_h)$ for the continuous data layers as discussed in Chung (2006).

The estimation of $\lambda(p{:}x_1,\cdots, x_k)$ is based on the ratios of two $c_1\times c_2\times\cdots\times c_k$ empirical cross-classified contingency tables (or thematic frequency tables: TFTs) (c_j is the number of categories in the j-th categorical variable), one for **M** and the other for $\overline{\mathbf{M}}$, and the empirical estimation of $\lambda(p{:}y_1,\cdots, y_h)$ is based on the ratios of two empirical frequency distribution functions (EDFs) using the kernel method (Silverman, 1986) (Fig. 3).

The estimation of Eq. (3) corresponds to:

$$\hat{\lambda}(p: x_1,\cdots,x_k,y_1,\cdots,y_h) = \hat{\lambda}(p: x_1,\cdots,x_k)\cdot\hat{\lambda}(p: y_1,\cdots,y_h) \quad (4)$$

where $\hat{\lambda}(p: x_1,\cdots,x_k)$ is an estimate of $\lambda(p{:}x_1,\cdots, x_k)$, and $\hat{\lambda}(p: y_1,\cdots,y_h)$ is an estimate of $\lambda(p{:}y_1,\cdots, y_h)$. The values of $\hat{\lambda}(p: x_1,\cdots,x_k,y_1,\cdots,y_h)$ may range $[0, \infty)$. According to the model, the pixel with the largest estimated value is considered to be the location most likely to be affected by future landslide reactivations. Using the estimate value of

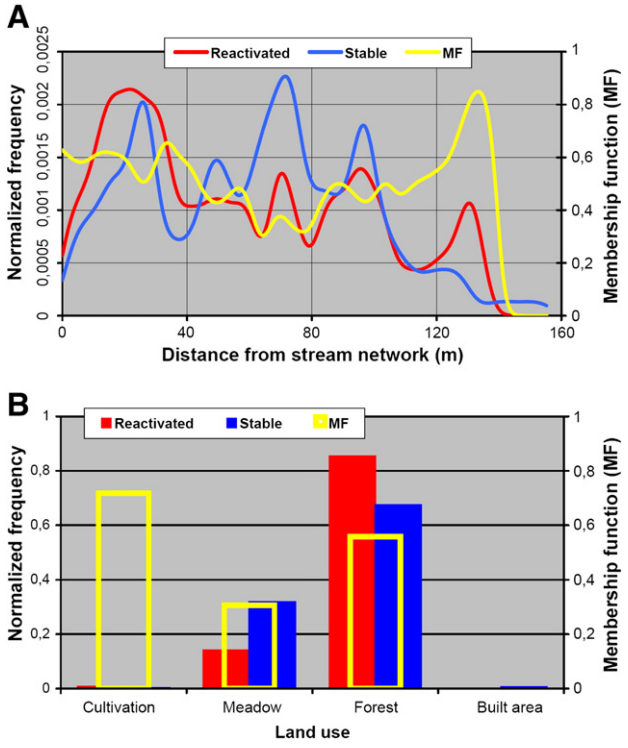

Fig. 3. Examples, for the study area, of empirical distribution functions (EDFs) and thematic frequency tables (TFTs) with their respective membership functions (MF). To give a membership value to each pixel of each input data layer we need to extract a pair of EDFs (or TFTs), one for the reactivated scarps and the other for the stable scarps. The EDF is determined using the normal density function as a kernel (Silverman, 1986), where a spread parameter equalling 2% of the total range of the input pixel values is applied. (A) EDFs calculated for the "distance from stream network" independent variable and the respective membership function computed with Eq. (7). (B) TFTs calculated for the "land use" independent variable and the respective membership function computed with Eq. (7). Both data layers used in the examples are from 1952.

the favourability function, a prediction map is generated, showing the susceptibility level on a continuous scale at every pixel in the map.

Chung and Fabbri (2008) defined the following function $\boldsymbol{\mu}$:

$$\boldsymbol{\mu}\{p : x_1,\cdots,x_k,y_1,\cdots,y_h\} = \frac{\mathbf{h}\left(\hat{\lambda}(p : x_1,\cdots,x_k,y_1,\cdots,y_h)\right)}{1+\mathbf{h}\left(\hat{\lambda}(p : x_1,\cdots,x_k,y_1,\cdots,y_h)\right)} \quad (5)$$

where $\mathbf{h}$ is an order-preserving function ($\mathbf{h}(a)\leq\mathbf{h}(b)$ if $a\leq b$). The range of $\boldsymbol{\mu}\{p:x_1,\cdots, x_k, y_1,\cdots, y_h\}$ is [0, 1]. Eq. (5) can be considered as a fuzzy membership function for the fuzzy set containing sub-areas likely to be affected by the future landslides. The idea behind fuzzy set theory is to consider how much a spatial object belongs to a set. In classical set theory, an object belongs or does not belong to a set which contains only 0 and 1 values as degrees of membership. In the fuzzy set theory, membership can take on any continuous value in the real number interval [0, 1], reflecting the degree of membership. When the degree of membership reaches 1, the element completely belongs to the set. Lower degrees express a partial membership to the set, down to the value of 0 which indicates no-belonging. A fuzzy set can thus be explained as a set containing elements that have varying degrees of membership in the set (Zimmermann, 1991; Klir and Yuan, 1995). The pixel with the largest estimate near 1 is considered to be the location most likely to be affected by future landslides.

Instead of considering m-dimensional multivariate distribution functions and under the conditional independence assumption, the likelihood ratio function may be estimated as a multiple of separate univariate likelihood ratio functions (Chung, 2006). Consider EDF-R, the empirical distribution function (or thematic frequency table) of the reactivated areas, and $\overline{EDF{-}NR}$, the respective empirical distribution function (or thematic frequency table) of the non-reactivated (stable) areas. Based on Eqs. (2) and (4), we get for one predictor variable the following univariate ratio function:

$$\hat{\lambda}(p : p_j) = \frac{EDF{-}R}{\overline{EDF{-}NR}} \quad (6)$$

Considering Eq. (6) in the estimate of Eq. (5) for one predictor variable and simplifying the resulting equation without considering an order-preserving function, we finally get the following membership function:

$$\boldsymbol{\mu}\left\{p : p_j\right\} = \frac{EDF{-}R}{EDF{-}R+\overline{EDF{-}NR}} \quad (7)$$

A membership value is therefore given to each pixel of each input data layer (Fig. 3). A variety of operators can be employed to combine the membership values (Zimmermann, 1991; Bonham-Carter, 1994; Moon, 1998). As already performed in several studies (e.g., Chung and Fabbri, 2001; Pistocchi et al., 2002; Tangestani, 2004; Lee, 2007), we applied the fuzzy Gamma operator which is defined as a combination of the fuzzy algebraic product and the fuzzy algebraic sum (Zimmermann,

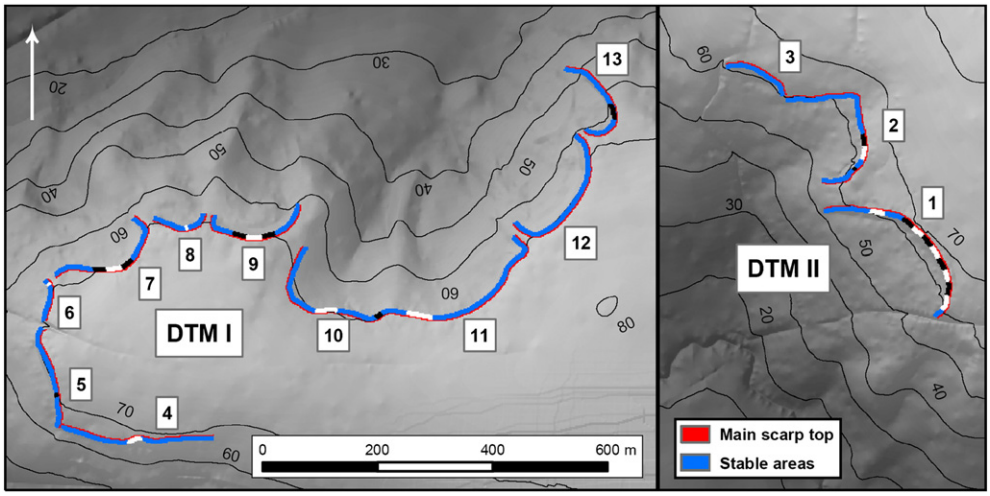

Fig. 4. Study area with the 26 occurrences of slope instability (or reactivation event) along the 13 landslide scarps used for the prediction validation. The occurrences (black and white areas) are presented with the 1952 topography that corresponds to the pre-reactivation conditions.

Table 2
Rotated factor matrix with absolute factor loadings over 0.7 in bold. The four factors explain 66.1% of the variance.

Variable	Factor 1	Factor 2	Factor 3	Factor 4
Elevation	**0.916**	0.011	−0.060	0.019
Slope angle	0.562	−0.034	0.034	0.130
Slope aspect-NS[a]	0.141	−0.042	−0.034	**−0.931**
Slope aspect-EW[b]	−0.050	0.025	0.049	**0.954**
Flow accumulation	−0.069	−0.052	**−0.951**	0.004
Focal flow	−0.041	−0.639	0.012	0.003
Profile curvature	0.051	**0.775**	−0.009	0.179
Planform curvature	−0.031	**0.848**	0.021	0.008
Distance from stream network	0.634	0.128	0.090	−0.204
Distance from cultivation	**−0.793**	0.036	0.095	0.304
Distance from Aalbeke Member	0.016	−0.319	−0.139	0.203
Vegetation index	0.063	−0.032	**−0.949**	−0.067
Total variance (%)[c]	18.5	15.5	15.4	16.7

[a] North–south component of slope aspect.
[b] East–west component of slope aspect.
[c] Portion of the variance explained by factor.

Table 3
Association between the reactivations and the predictor variables. Cramer's V values in bold are the variables selected for Model Chi-2.

Variable	Chi-2	Cramer's V
Elevation	257.3	**0.232**
Slope angle	481.6	**0.277**
Slope aspect	1093.0	**0.416**
Flow accumulation	67.8	0.104
Focal flow[a]	6.9	0.033
Profile curvature	61.9	0.099
Planform curvature[a]	25.4	0.064
Distance from stream network	175.6	0.167
Land use	55.6	0.094
Lithology	55.6	0.094
Distance from cultivation	455.2	**0.268**
Distance from Aalbeke Member	363.1	**0.240**
Vegetation index	28.5	0.067

[a] Predictor variable not significant (significance level = 0.05).

1991). The joint membership function at a pixel is defined as:

$$\boldsymbol{\mu}(x) = \left[\mu_{\text{product}}(x)\right]^{1-\gamma}\left[\mu_{\text{sum}}(x)\right]^{\gamma} \quad (8)$$

where γ is a constant parameter chosen in the range [0, 1]. The fuzzy algebraic product and fuzzy algebraic sum are calculated using the following equations, respectively:

$$\mu_{\text{product}}(x) = \left[\prod_{j=1}^{m} \mu_j(x)\right] \quad (9)$$

$$\mu_{\text{sum}}(x) = \left[1 - \prod_{j=1}^{m} \left(1-\mu_j(x)\right)\right] \quad (10)$$

where $\mu_j(x)$ is the fuzzy membership function for the j-th map, and $j = 1, 2, \cdots, m$ are the maps that have to be combined for the prediction. The Gamma operator is a useful tool for calculating a range of values going from a minimum, corresponding to the algebraic product ($\gamma = 0$), to a maximum, corresponding to the algebraic sum ($\gamma = 1$). Though it has been shown that fuzzy operators may depend on the type of spatial data (Moon, 1998), we decided to use here only the Gamma operator with $\gamma = 0.5$. This choice of value ensures a compromise between the "decreasing" effects of the fuzzy algebraic product and the "increasing" effects of the fuzzy algebraic sum. The estimator of Eq. (8) can be used to describe the susceptibility attached to the pixel.

4.2. Data combination

Several data combinations will be analysed with regard to geomorphological and quantitative criteria. A drawback of our modelling approach lies in the conditional independence assumption made among the predictor variables that requires that each factor provides "independent" evidence for the occurrence of future landslides. This may cause the spatial probabilities to be either overestimated or underestimated (Bonham-Carter, 1994). To quantify the possible correlation between the factors, a Principal Component Analysis (PCA) will be performed (e.g., Baeza and Corominas, 2001; Santacana et al., 2003). PCA provides some insights on the structure of the overall population, and knowing how the population is structured may allow the identification of variables having similar behaviour and to detect correlation that is difficult to observe with a simple correlation matrix. This allows a selection of the most significant variables.

Data selection will also rely on Chi-square (Chi-2) statistics to test the association between each predictor variable and the occurrence of slope instabilities. The Cramer's V statistics, based on the Chi-2 values, will be applied to test the strength and the type of the association (Bonham-Carter, 1994). Chi-2 values correspond to an absolute measure of the association and are useless in themselves, while V index gives a standardized values ranging between 0 and 1. The closer V is to 1, the stronger is the association between two variables.

4.3. Validation procedure

The validation of the result is a mandatory step to assess the accuracy and the reliability of a model (Chung and Fabbri, 2003; Brenning, 2005; Guzzetti et al., 2006). Time partitioning of landslide occurrences is the most natural and convincing strategy to validate a prediction image for future events. In our research, because only one time interval of past occurrence is available, a spatial partitioning was performed. The field observation of recent reactivations in the study area (Van Den Eeckhaut et al., 2007b; Dewitte et al., 2008, 2009) and other reactivations in the Flemish Ardennes (Dewitte, 2006) attest that such movements, when they occur, do not affect the whole length of the scarp in one time. Large reactivated areas, as the one of landslide 1 (Fig. 2), instead result from successive collapses. It is also observed that the whole height of the scarp is at each time affected by a reactivation. With regard to these observations, the 14 reactivated parts detected along the scarps (Fig. 2) were manually divided into 26 scarp segments of similar length (~20 to 30 m) that we consider to correspond to the unit length of a reactivation event (Fig. 4). Through this segmentation, we need to consider the spatial autocorrelation between the pixels of an individual movement since, when a reactivation occurs, cells within it move together. Such a segmentation is obviously related to uncertainties, like for common delimitation of landslide boundaries (Malamud et al., 2004; Galli et al., 2008), but it does not modify the real proportion of the study area affected by the reactivations.

The prediction rate of the resulting susceptibility map is estimated by a spatial cross-validation procedure sequentially excluding some reactivated scarp segments at random. The random selection of observations also helps to circumvent the potential risks of spatial autocorrelation (Diniz-Filho et al., 2003). To evaluate the prediction results, we applied the procedure proposed by Dewitte et al. (2006). We first remove randomly 2 of the 26 reactivated scarp segments as if they had not yet occurred. Then, using the remaining 24 occurrences, a susceptibility model is computed based on the estimator of Eq. (8). The favourability indices (or joint membership values) obtained in the two occurrences not used in the modelling are appraised and the prediction of one occurrence is considered successful when at least 25% of it (i.e. 25% of its pixels) lie within the part of the study area that is predicted as being the most susceptible to reactivation. In other words, we then obtained for each of the occurrences an individual prediction rate that indicates how many percents of the study area (the pixels being ranked decreasingly) have to be selected in order to include 25% of this instability in the hazardous area.

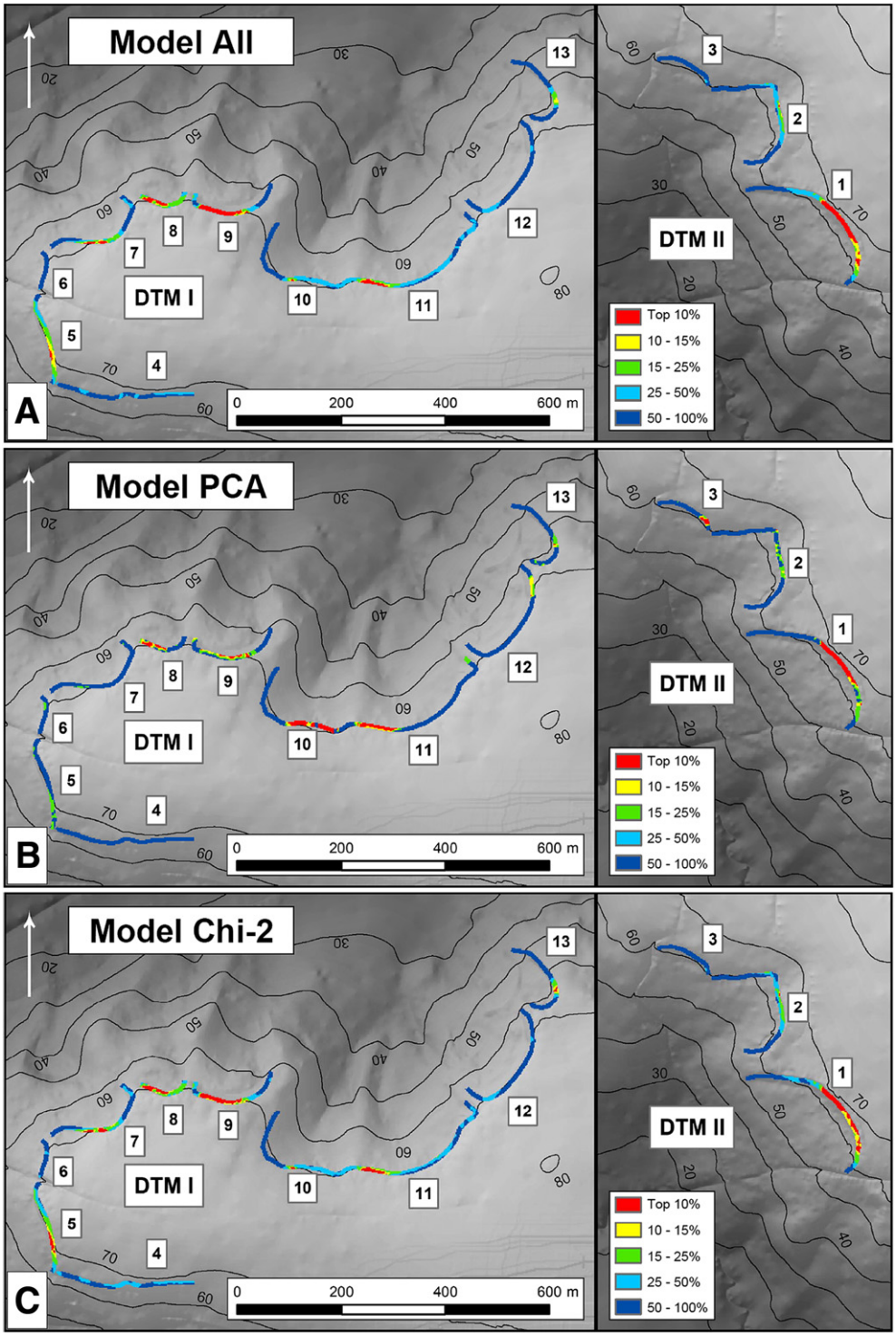

Fig. 5. Susceptibility maps of the scarp reactivation obtained from the 1952 data layers. The pixels are ranked according to their degree of susceptibility (joint membership value). The top 10% most hazardous pixels are distinguished in red. (A) Model All using the 13 predictor variables. (B) Model PCA using elevation, planform curvature, flow accumulation and slope aspect. (C) Model Chi-2 using slope aspect, slope angle, distance from cultivation, distance from Aalbeke Member and elevation. (D) Model Empi using slope aspect, planform curvature, vegetation index and focal flow. (E) Model Expert using slope angle, flow accumulation, elevation and distance from cultivation.

This experiment is repeated 13 times in order to consider only once each of these 26 occurrences. The prediction-rate curves associated with a prediction is plotted from these 26 values. For each curve, the smallest portion necessary to predict an occurrence is first placed on the *x*-axis with its corresponding reactivated area on the *y*-axis. Afterwards, the second smallest portion value is plotted on the graph and the second *y* value equals the cumulative reactivated areas, etc.

A critical point in our validation methodology is the use of a value of only 25% for the estimation of the prediction rates, whereas a value of at least 50% may be more realistic. In the susceptibility mapping literature, a landslide is commonly considered as one single occurrence that develops in one time. Such an assumption can be realistic for a small landslide, but can be inappropriate for a large rotational landslide for which the surface extent is often the result of a succession of movements, as it is notably

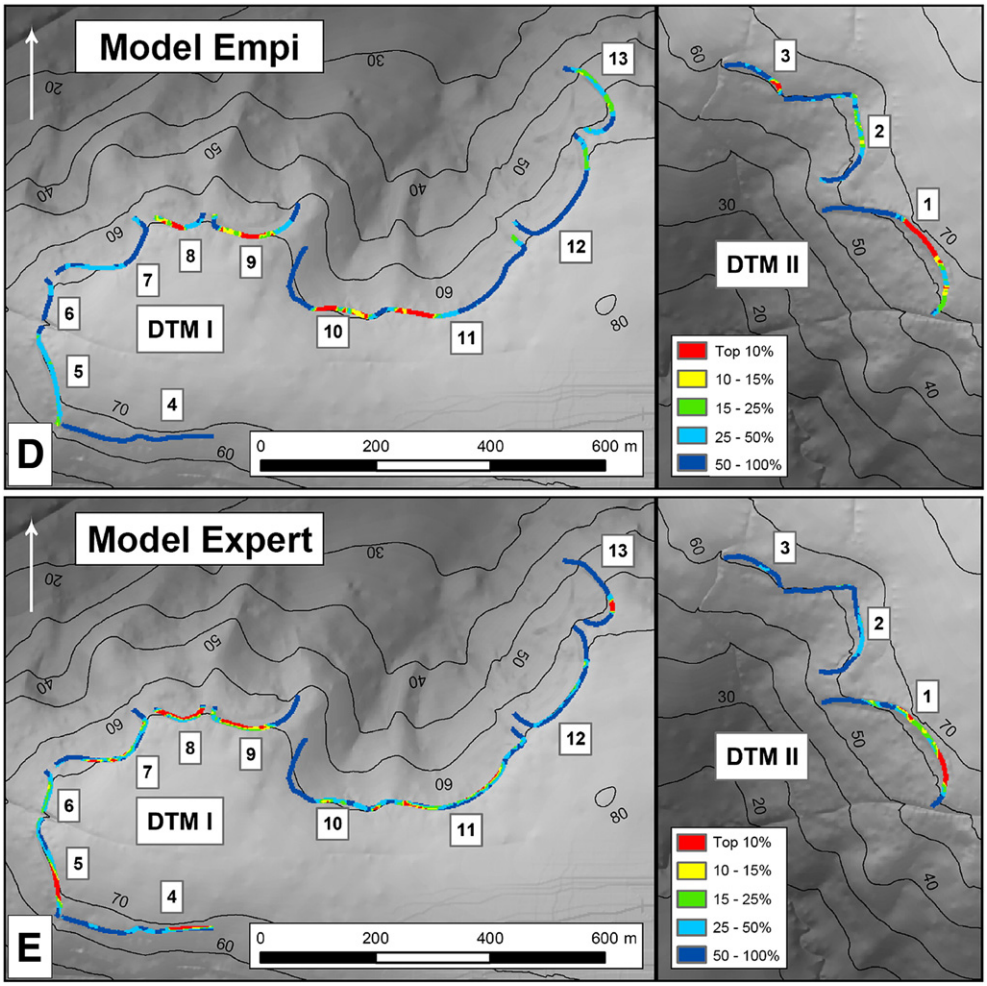

Fig. 5 (*continued*).

demonstrated for the Flemish Ardennes (Van Den Eeckhaut et al., 2007a; Dewitte et al., 2009). In this case study, we use reactivated segments with the knowledge that, when a reactivation occurs, the whole height of the scarp is affected in one time. This allows us to better define the reality of the slope processes. Based on the comparison of several tests performed with both 50% and lower values, it was then decided that using 25% was a good balance between the geomorphological aspect and the improvement of the model performance (Dewitte, 2006).

Without this cross-validation procedure, the susceptibility maps cannot be quantitatively evaluated and therefore would be meaningless. Moreover, it provides support for the model comparison and the evaluation of the contribution of each input layer to the prediction.

5. Results

5.1. Data combinations

We tested five data combinations:

- Model All: the 13 independent conditioning variables
  This combination includes all the spatial data supposed to control the landslide reactivation and considered relevant for the susceptibility mapping.
- Model PCA: elevation, planform curvature, flow accumulation and slope aspect
  This combination includes the variables that are the most representative of each component resulting from a PCA applied on the continuous predictor variables. Due to the circular nature of slope aspect, we considered it in the PCA as two variables corresponding to its north–south and east–west components. PCA was performed with standardised variables (i.e. the variance of each variable = 1 so that the total variance of the continuous variables = 12). Table 2 presents the rotated matrix with the factors with an eigenvalue > 1. It stresses that more than 66% of the variance of the continuous predictor variables can be expressed by four factors. Weightings of the factor show that each factor is mainly defined by two variables; each of the two contributes about the same.

Factor 1 represents the elevation component. The variable "distance from cultivation" is related to "elevation" and logically of opposite sign because it is calculated from the cultivations located upslope of the main scarp. The correlation between "slope angle" and "elevation" is explained by the presence of the highest slope angles along the highest parts of the main scarps (Dewitte, 2006).

Variables planform and profile curvatures and to a lesser extent focal flow define the second factor while flow accumulation and the vegetation index define factor 3. Slope aspect is clearly associated with factor 4.

PCA can have difficulties in dealing with categorical data and optimal results are not guaranteed (Dillon and Goldstein, 1986). Therefore, both categorical variables land use and lithology were not included in the analysis. They could have been considered as binary variables (4 for land use and 3 for lithology), but their relative contribution on the total variance (7 and 19 respectively) produced unreliable results (Dewitte, 2006). Chi-2 tests applied between the two categorical data and the four main components revealed a significant association with the four factors, more particularly with factors 1 and 4 (Dewitte, 2006).

From PCA, a dataset with the most significant variable of each factor was taken as a susceptibility model: elevation for factor 1, planform curvature for factor 2, flow accumulation for factor 3, and slope aspect for factor 4.

- Model Chi-2: slope aspect, slope angle, distance from cultivation, distance from Aalbeke Member and elevation
  Chi-2 and Cramer's V statistics (e.g., Pistocchi et al., 2002; Van Den Eeckhaut et al., 2006; Thiery et al., 2007) were applied for the selection of the variables of this model (Table 3). It includes the five variables with the highest Cramer's V value. Slope aspect has the highest predictive power. Due to the very small difference between "distance from Aalbeke Member" and "elevation", we chose five variables in spite of four as pointed out in the PCA.
- Model Empi: slope aspect, planform curvature, vegetation index and focal flow
  This combination was obtained through an empirical selection of the variables (Dewitte, 2006). Based on the prediction rate of each individual variable obtained by applying Eq. (8) and the above-mentioned cross-validation procedure, we selected the best factor to predict landslide occurrence. Then we tested all the possible pairs of variables including this factor and, on the basis of the prediction rate again, selected the best two-variable model. By successively adding a variable to the precedent best model until having the best prediction rate, we obtained a four data layers model (Dewitte et al., 2006). Slope aspect is the variable with the highest predictive power when considered individually.
- Model Expert: slope angle, flow accumulation, elevation and distance from cultivation
  The selection of the predictor variables of the Model Expert relies on our expertise in the field and the information collected over the last 50 years (Van Den Eeckhaut et al., 2007b; Dewitte et al., 2008, 2009). This combination includes the four variables that were considered as having the biggest impact on the reactivation process. To consider the occurrence of a perched water table in relation with the presence of the Aalbeke clays, we chose elevation which has a higher accuracy than lithology and distance to Aalbeke Member.

5.2. Susceptibility mapping based on the 1952 data

The 1952 models were built from the relations linking the 1952–1996 scarp retreat events to the conditioning parameters of 1952. There is an uncertainty associated with the thematic data, so that they have characteristic fuzzy boundaries. This was taken into account in the prediction by defining β as the radius in terms of numbers of pixels, which corresponds to the likely uncertainty of boundaries in the layers (Chung, 2006). If $\beta=1$, the value of each pixel contained in the thematic layer will be preserved. If $\beta>1$, the value of each pixel contained in a buffer of a width $=2\beta$ around the boundaries has to be modified. Suppose a circle with a radius $\beta>1$ drawn at the centre of pixel in the thematic layer, this circle containing several pixels of different values. The new value of the pixel of the boundary corresponds to the sum of the products of each pixel value multiplied respectively by the portion of the area occupied by the corresponding pixel value within the circle. β is a function of the original map scale, the pixel resolution, and the subjective interpretation of the original data by the cartographer. For the predictor variables land use and lithology, an uncertainty of respectively 3 m and 50 m was estimated (Dewitte, 2006). We therefore considered $\beta=1$ and $\beta=12$ in the modelling.

The prediction maps were obtained by applying Eq. (8). The computed values of Eq. (8), which may range from 0 to 1, were sorted in decreasing order (the pixel with the largest estimator is given the highest order). The membership value estimated at each pixel was replaced by its rank divided by the total number of pixels. Therefore, rather than the values of the estimator of Eq. (8), we used their standardised ranks to generate a susceptibility map. They were grouped into 200 classes, so that each class covers 0.5% of the total study area (thus contains 0.5% of the total number of pixels in the study area) (Chung, 2006; Dewitte et al., 2006). The maps computed from the five data combinations predict the susceptibility to reactivation for each pixel (Fig. 5).

The prediction-rate curves obtained for the five maps are shown in Fig. 6. The steeper the curve, the higher the prediction power of the map. For Model Empi, 20% of pixels with the highest favourability indices suffice to define the areas where 60% of future reactivation is expected to occur. After this point, the slope of the curve is globally lower than the black dashed line (slope = 1) and hence it has less significance. This prediction-rate curve is then less usable for the interpretation of all the classes beyond the hazardous class with the value of 20%. At this value of 20%, the other models are less successful. Model PCA predicts just below 50% and Model Chi-2 ~45%.

If we consider the portion of the most hazardous percent of the study area to be selected to predict at least 50% of the future movements (i.e. better than a randomly prediction is supposed to provide), Model Empi, with 18%, is the most relevant. Then come Models PCA and Chi-2, with 23%, and finally Models All and Expert around 35% (Fig. 6).

Thanks to the validation we get a quantitative estimate of the ability of the models to predict correctly the spatial occurrence of new reactivations. It however gives no clue on how realistic these maps are and there is no way to choose between various models other than to invoke heuristic reasons (Oreskes et al., 1994). We therefore considered two geomorphological criteria to evaluate the reliability of the prediction maps: (1) the similarity between the location of the highest susceptibility areas and the location of the reactivations that were detected in the study area between 1952 and 1996, and in

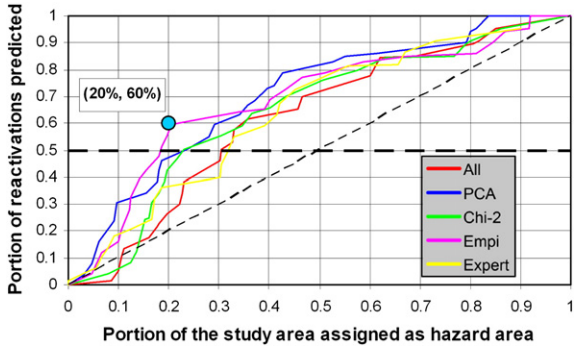

Fig. 6. Prediction-rate curves obtained by cross-validation for the five 1952 susceptibility maps of Fig. 5. These cumulative plots indicate how many "most hazardous" percents of the study area (x-axis) have to be taken into account to predict a given percentage of the future reactivations (y-axis) according to each model and the adopted cross-validation process. For Model Empi, the highest hazardous 20% of the study area contain 60% of the predicted reactivations (blue point). The black horizontal dashed line (slope = 0) represents 50% of the predicted reactivations. The black dashed line (slope = 1) represents a curve for a "randomly" constructed prediction.

Table 4
Qualitative evaluation of the geomorphological reliability of the susceptibility maps presented in Fig. 5. See text for explanation on the two criteria.

Susceptibility map	Criterion 1*		Criterion 2	
Model All	Good	3**	Not good	4
Model PCA	Good	3	Good	3
Model Chi2	Very good	1	Good	2
Model Empi	Good	2	Very good	1
Model Expert	Good	5	Not good	5

*Similarity with the criterion.
**Hierarchy of the maps (1 = the best).

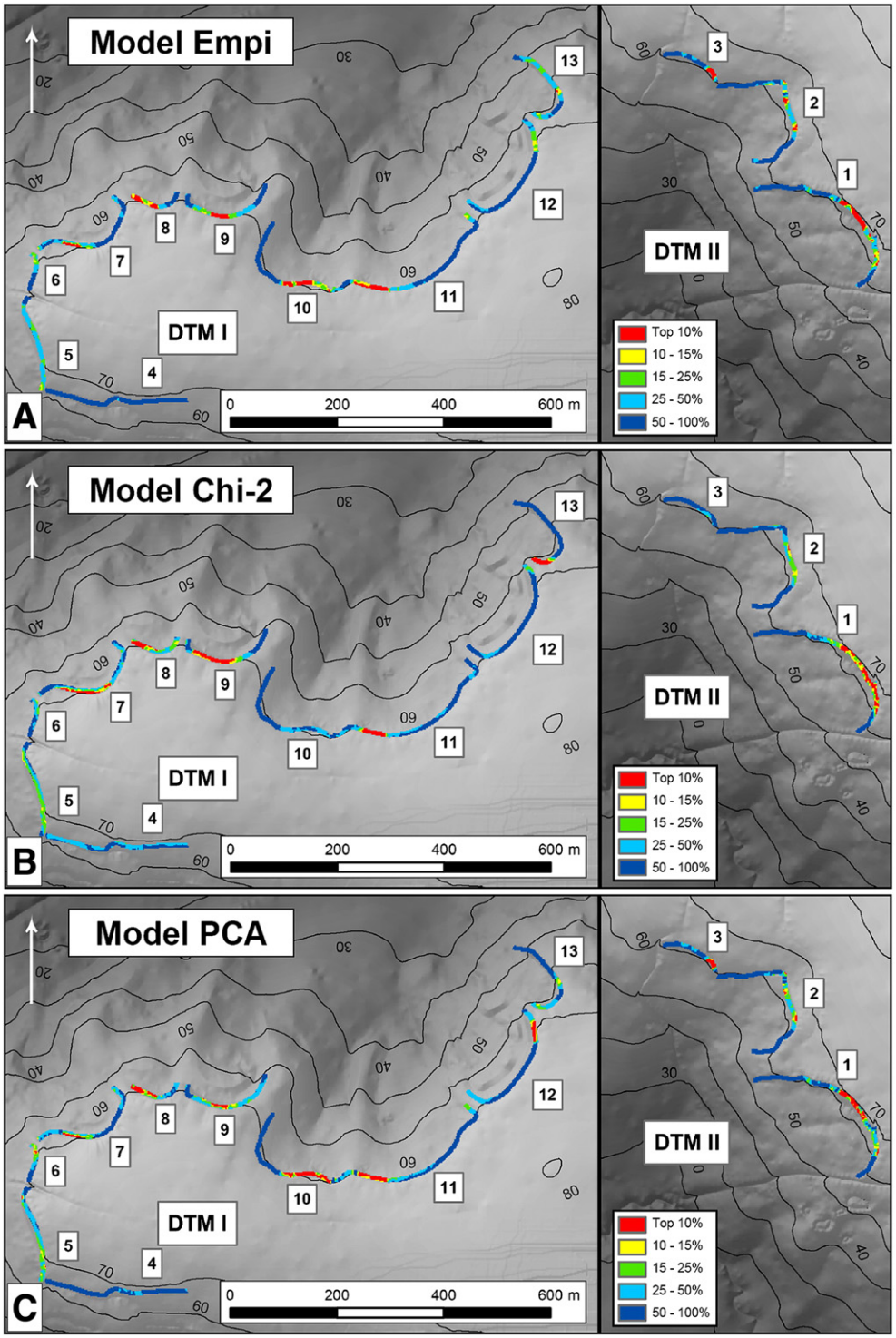

Fig. 7. Susceptibility maps of the scarp reactivation obtained from the 1996 data layers with the statistics of the 1952 models. The pixels are ranked according to their degree of susceptibility (joint membership value). The top 10% most hazardous pixels are distinguished in red. (A) Model Empi using slope aspect, planform curvature, vegetation index and focal flow. (B) Model Chi-2 using slope aspect, slope angle, distance from cultivation, distance from Aalbeke Member and elevation. (C) Model PCA using elevation, planform curvature, flow accumulation and slope aspect.

particular those who have affected landslide 1 since February 1995 (Dewitte et al., 2008, 2009); and (2) the similarity between the shape of the highest susceptibility areas (top 10%) and the recent movements that were observed. At each time, a reactivation affects the whole height of the scarp. Considering that the main objective of a prediction is to locate the place of a future instability, we paid more attention to criterion 1. Table 4 gathers the qualitative evaluation of the five maps. According to our criteria, maps produced by the Models Empi and Chi-2 provide the best results whereas the predictions of Models Expert and All result in less reliable values, especially when criterion 2 is considered. However, arguing that a model would be less convenient for a prediction is too early at this step of the research.

Based on both the quantitative and qualitative criteria, the three models being the most relevant are Models Empi, Chi-2 and PCA. According to the same criteria, Model Expert is the less adapted.

5.3. Susceptibility mapping based on the 1996 data

We applied the statistics of the models computed for 1952 (Models Empi, Chi-2 and PCA) to the conditioning variables of 1996 to produce the susceptibility maps responding to more recent conditions (Fig. 7). In fact, each pixel value of each predictor variables of 1996 was not used as such in the prediction but replaced by a membership value derived directly from those computed with Eq. (7) for each variables of 1952. Eq. (8) was then applied to the weighted 1996 data layers for producing the three prediction maps presented in Fig. 7. Except for landslide 1 where post-1996 movements associated with the reactivation of its main scarp were measured (Dewitte et al., 2008), no other quantitative information on reactivations developed after this period is available. We therefore have no quantitative means to validate these maps. However, as the study area of 1996 is very similar to that of 1952, the reliability of the 1996 predictions should be approximately the same.

Based on field observations and notably the reactivations that occurred after 1996 in the study area (i.e. those of landslide 1; Dewitte et al., 2008), Models Empi and PCA look the most adapted for the prediction.

6. Discussion

6.1. Geomorphological significance of the predictions

Although the reactivations observed in landslide 1 from 1995 to the present time have been better predicted by Models Empi and PCA, we remain cautious in stating that one model is closer to the geomorphological reality than the other. The modelling allows however some geomorphological issues to be discussed. It highlighted the importance of surface runoff and its relation to the vegetation cover. Both Models Empi and PCA as well as Chi-2 consider surface runoff through either direct (variables flow accumulation, focal flow and planform curvature) or proxy (vegetation index and distance from cultivation) indicators. The significant role of surface runoff upslope of the main scarp and the presence of cultivations was notably evidenced for landslide 1 reactivation (Dewitte et al., 2008, 2009). The effect of the heavy rainfall at the origin of this reactivation was enhanced by increased surface runoff resulting from the presence of cultivated parcels that expose bare soils in winter.

The models also point out the influence of slope aspect which appears here as one of the most relevant conditioning factors. Slope aspect exerts an effect over the rainfall amounts brought by the dominant winds and to a lesser extent the solar radiation which influences soil humidity. Despite a low relief and quite a smooth topography, the marginal environmental differences related to this parameter seem to have a higher impact than initially expected (this explains why we did not select it for Model Expert).

Contrary to the surface water concentration, the groundwater conditions reflected by the elevation factor and to a less extent by the distance from Aalbeke Member were not really put forward. This suggests that runoff might prevail over percolation in favouring reactivation, which could be true when bare (cultivated) soils undergoing winter rainfall extend close to the scarp.

The reliability of the variables is also a critical point as it may question the geomorphological significance of a model. A variable can be crucial to model the process and it can be useless because of the quality. As pointed out in Section 3, flow accumulation is the only parameter in our database where we expect that topographic data errors can affect its reliability. We agree that these errors can lead to different susceptibility values from one pixel to the other. However, since the pattern of flow accumulation is not really affected by the errors, and since the evaluation of the models is based on areas of susceptibility, notably through the use of scarp segments, we can consider that the geomorphological significance of the models is preserved.

Even if the dataset used in our predictions is quite large with regards to what is commonly used for the researches on landslide mapping, we acknowledge that the model performance can always be improved with the support of additional information. For example, it is widely recognized that groundwater conditions are of paramount importance in the process of slope stability (Van Asch et al., 1999; Iverson, 2000). Groundwater data can however be difficult to obtain, especially when information on their spatial variability is required (Luzi et al., 2000; Ohlmacher and Davis, 2003). In our model, the elevation data were used to appraise these conditions.

6.2. Landslide triggering factors

A drawback of many indirect mapping methods is the tendency to simplify the factors that condition landslides by only taking those that can be easily mapped (Van Westen et al., 2003, 2006). The high resolution of the DTMs allowed us to generate all the potentially predisposing factors that we supposed to affect the slope stability. We however did not take any triggering factor into account. Precipitation is the main triggering factor for the reactivation (Dewitte et al., 2009). However, due to the spatial proximity of the two investigated hills and the close similarity of their relief, the spatial variation of this factor is very low and therefore did not deserve any special attention. Reactivations might also be triggered by factors associated with seismic shaking. We however do not have any clue about that and for the same reasons of spatial proximity and topographic similarity we did not include this factor in the prediction. The geomorphological analysis of the ground displacements that occurred during the last 50 years within the studied landslides did not reveal human activity as a triggering factor of the scarp reactivations (Dewitte et al., 2009).

6.3. Conditional independence

The predictive modelling requires that each controlling factor provides “independent” evidence for future occurrences. The idea behind PCA was to help in the selection of a combination of variables with the lowest possible correlation among them. It however does not mean that these variables are fully independent. To examine the effect of violation of the assumption of conditional independence among the predictor variables, we tested two additional data combinations. We entered twice the slope aspect in Model PCA and twice the vegetation index in Model Empi to simulate the use of two non-independent variables and then generated two prediction maps similar to those in Fig. 5. Although the assumption of conditional independence was clearly violated in both experiments, the prediction maps based on five rather than four data layers (not shown) were essentially unchanged (Dewitte, 2006). As pointed out by Chung (2006) and Chung and Fabbri (2008), a reason for the robustness is that the membership functions themselves are not interpreted; instead, the relative rankings of the predicted membership function scores are used to predict the level of susceptibility. In practice, correlations among variables would not be as severe as in these two experiments. Even though some degree of violation of the independence assumption is expected in real situations, these violations should not significantly alter class patterns in the prediction maps.

7. Conclusions

In this study conducted on the main scarps of 13 landslides in W Belgium, the chosen likelihood ratio approach has shown to be efficient at yielding relevant maps for predicting the susceptibility to scarp reactivation at a 2 m-resolution. Our pixel-based research leads to the following conclusions:

1) There is a need for testing several data combinations in a landslide prediction, especially when the availability of high-resolution data

makes it possible for the consideration of a wide range of potential predictor variables. Throughout all these procedures, validation is a mandatory step.

2) A careful balancing of geomorphologist's expertise and the objectivity of statistical treatment is a key issue to obtain accurate landslide susceptibility maps. To this end, using the modelling with both a predictive and an inductive goal is an asset. A purely mathematical treatment can be misleading and leads to unrealistic prediction whereas a purely heuristic approach can be too subjective.
3) For this case study, there is an optimal set of information for the prediction (four or five data layers out of 13). This provides an example of the concept of "optimum model complexity" exposed by Grayson et al. (2002) that describes the relationship among data availability, model complexity, and predictive performance of the model. For a given model complexity, increasing data availability improves the predictive performance up to a point, after which a decreasing model performance is observed. According to Glade and Crozier (2005), this relation is due to the fact that a model with a given complexity can only be used to predict a data set of a given quality. Adding data in a combination does not systematically improve the prediction.

References

Akgun, A., Dag, S., Bulut, F., 2008. Landslide susceptibility mapping for a landslide-prone area (Findikli, NE of Turkey) by likelihood-frequency ratio and weighted linear combination models. Environmental Geology 54, 1127–1143.

Atkinson, P.M., Massari, R., 1998. Generalised linear modelling of susceptibility to landsliding in the central Apennines, Italy. Computers and Geosciences 24, 373–385.

Baeza, C., Corominas, J., 2001. Assessment of shallow landslide susceptibility by means of multivariate statistical techniques. Earth Surface Processes and Landforms 26, 1251–1263.

Bonham-Carter, G.F., 1994. Geographic Information System for Geoscientists: Modelling with GIS. : Computer Methods in the Geosciences, 13. Pergamon, New York (398 pp.).

Brenning, A., 2005. Spatial prediction models for landslide hazards: review, comparison and evaluation. Natural Hazards and Earth System Sciences 5, 853–862.

Chang, K.T., Tsai, B.W., 1991. The effect of DEM resolution on slope and aspect mapping. Cartography and Geographic Information Systems 18, 69–77.

Chung, C.J., 2006. Using likelihood ratio functions for modeling the conditional probability of occurrence of future landslides for risk assessment. Computers and Geosciences 32, 1052–1068.

Chung, C.F., Fabbri, A.G., 2001. Prediction models for landslide hazard using a fuzzy set approach. In: Marchetti, M., Rivas, V. (Eds.), Geomorphology and Environmental Impact Assessment. A. A. Balkema, Rotterdam, pp. 31–47.

Chung, C.F., Fabbri, A.G., 2003. Validation of spatial prediction models for landslide hazard mapping. Natural Hazards 30, 451–472.

Chung, C.F., Fabbri, A.G., 2005. Systematic procedures of landslide-hazard mapping for risk assessment using spatial prediction models. In: Glade, T., Anderson, M.G., Crozier, M.J. (Eds.), Landslide Hazard and Risk. Wiley, Chichester, pp. 139–174.

Chung, C.J., Fabbri, A.G., 2008. Predicting landslides for risk analysis — spatial models tested by a cross-validation technique. Geomorphology 94, 438–452.

Dai, F.C., Lee, C.F., Ngai, Y.Y., 2002. Landslide risk assessment and management: an overview. Engineering Geology 64, 65–87.

Demoulin, A., Chung, C.J., 2007. Mapping landslide susceptibility from small datasets: a case study in the Pays de Herve (E Belgium). Geomorphology 89, 391–404.

Dewitte, O., 2006. Kinematics of landslides in the Oudenaarde area and prediction of their reactivation: a probabilistic approach. Ph.D. Thesis, University of Liège, Liège, 213 pp.

Dewitte, O., Demoulin, A., 2005. Morphometry and kinematics of landslides inferred from precise DTMs in West Belgium. Natural Hazards and Earth System Sciences 5, 259–265.

Dewitte, O., Chung, C.-J., Demoulin, A., 2006. Reactivation hazard mapping for ancient landslides in West Belgium. Natural Hazards and Earth System Sciences 6, 653–662.

Dewitte, O., Jasselette, J.-C., Van Den Eeckhaut, M., Cornet, Y., Collignon, A., Poesen, J., Demoulin, A., 2008. Tracking landslide displacements by multi-temporal DTMs: a combined aerial stereophotogrammetric and LIDAR approach in western Belgium. Engineering Geology 99, 11–22.

Dewitte, O., Van Den Eeckhaut, M., Poesen, J., Demoulin, A., 2009. Decadal-scale analysis of ground movements in old landslides in Western Belgium. Zeitschrift für Geomorphologie 53, 23–45.

Dillon, W.R., Goldstein, M., 1986. Multivariate analysis. Methods and Applications. Wiley, Chichester. (565 pp.).

Diniz-Filho, J.A.F., Bini, L.M., Hawkins, B.A., 2003. Spatial autocorrelation and red herrings in geographical ecology. Global Ecology and Biogeography 12, 53–64.

Ercanoglu, M., Kasmer, O., Temiz, N., 2008. Adaptation and comparison of expert opinion to analytical hierarchy process for landslide susceptibility mapping. Bulletin of Engineering Geology and the Environment 67, 565–578.

Fell, R., Corominas, J., Bonnard, C., Cascini, L., Leroi, E., Savage, W.Z., 2008. Guidelines for landslide susceptibility, hazard and risk zoning for land-use planning. Engineering Geology 102, 99–111.

Florinsky, I.V., 1998. Accuracy of local topographic variables derived from digital elevation models. International Journal of Geographical Information Science 12, 47–61.

Galli, M., Ardizzone, F., Cardinali, M., Guzzetti, F., Reichenbach, P., 2008. Comparing landslide inventory maps. Geomorphology 94, 268–289.

Glade, T., Crozier, M.J., 2005. A review of scale dependency in landslide hazard and risk analysis. In: Glade, T., Anderson, M.G., Crozier, M.J. (Eds.), Landslide Hazard and Risk. Wiley, Chichester, pp. 75–138.

Grayson, R.B., Blöschl, G., Western, A.W., McMahon, T.A., 2002. Advances in the use of observed spatial patterns of catchment hydrological response. Advances in Water Resources 25, 1313–1334.

Guzzetti, F., Reichenbach, P., Ardizzone, F., Cardinali, M., Galli, M., 2006. Estimating the quality of landslide susceptibility models. Geomorphology 81, 166–184.

Hjort, J., Marmion, M., 2008. Effects of sample size on the accuracy of geomorphological models. Geomorphology 102, 341–350.

Iverson, R.M., 2000. Landslide triggering by rain infiltration. Water Resources Research 36, 1897–1910.

Jacobs, P., De Ceukelaire, M., De Breuck, W., De Moor, G., 1999. Text Clarifying the Belgian geological Map, Flemish Region, Map Shet 29 Kortrijk, Map Scale 1/50, 000 (in Dutch). Ministerie van Economische Zaken and Ministerie van de Vlaamse Gemeenschap, 68 pp.

Keefer, D.K., 1984. Landslides caused by earthquakes. Geological Society of America Bulletin 95, 406–421.

Klir, G.J., Yuan, B., 1995. Fuzzy Sets and Fuzzy Logic: Theory and Applications. Prentice Hall, New Jersey. (573 pp.).

Lee, S., 2007. Application and verification of fuzzy algebraic operators to landslide susceptibility mapping. Environmental Geology 52, 615–623.

Lee, S., Pradhan, B., 2007. Landslide hazard mapping at Selangor, Malaysia using frequency ratio and logistic regression models. Landslides 4, 33–41.

Lee, S., Ryu, J.H., Kim, I.S., 2007. Landslide susceptibility analysis and its verification using likelihood ratio, logistic regression, and artificial neural network models: case study of Youngin, Korea. Landslides 4, 327–338.

Luzi, L., Pergalani, F., Terlien, M.T.J., 2000. Slope vulnerability to earthquakes at subregional scale, using probabilistic techniques and geographic information systems. Engineering Geology 58, 313–336.

Malamud, B.D., Turcotte, D.L., Guzzetti, F., Reichenbach, P., 2004. Landslide inventories and their statistical properties. Earth Surface Processes and Landforms 29, 687–711.

Moon, W.M., 1998. Integration and fusion of geological exploration data: a theoretical review of fuzzy logic approach. Geosciences Journal 2, 175–183.

Nefeslioglu, H.A., Gokceoglu, C., Sonmez, H., 2008. An assessment on the use of logistic regression and artificial neural networks with different sampling strategies for the preparation of landslide susceptibility maps. Engineering Geology 97, 171–191.

Ohlmacher, G.C., Davis, J.C., 2003. Using multiple logistic regression and GIS technology to predict landslide hazard in northeast Kansas, USA. Engineering Geology 69, 331–343.

Oreskes, N., Shrader-Frechette, K., Belitz, K., 1994. Verification, validation, and confirmation of numerical models in the Earth Sciences. Science 263, 641–646.

Pistocchi, A., Luzi, L., Napolitano, P., 2002. The use of predictive modeling techniques for optimal exploitation of spatial databases: a case study in landslide hazard mapping with expert system-like methods. Environmental Geology 41, 765–775.

Poesen, J., Nachtergaele, J., Verstraeten, G., Valentin, C., 2003. Gully erosion and environmental change: importance and research needs. Catena 50, 91–133.

Regmi, N.R., Giardino, J.R., Vitek, J.D., 2010. Modeling susceptibility to landslides using the weight of evidence approach: Western Colorado, USA. Geomorphology 115, 2010.

Rossi, M., Guzzetti, F., Reichenbach, P., Mondini, A.C., Peruccacci, S., 2010. Optimal landslide susceptibility zonation based on multiple forecasts. Geomorphology 114, 129–142.

Santacana, N., Baeza, B., Corominas, J., De Paz, A., Marturia, J., 2003. A GIS-based multivariate statistical analysis for shallow landslide susceptibility mapping in La Pobla de Lillet area (Eastern Pyrenees, Spain). Natural Hazards 30, 281–295.

Silverman, B.W., 1986. Density estimation for statistics and data analysis. Monographs on Statistics and Applied Probability, 26. Chapman & Hall, London (200 pp.).

Tangestani, M.H., 2004. Landslide susceptibility mapping using the fuzzy gamma approach in a GIS, Kakan catchment area, southwest Iran. Australian Journal of Earth Sciences 51, 439–450.

Thiery, Y., Malet, J.P., Sterlacchini, S., Puissant, A., Maquaire, O., 2007. Landslide susceptibility assessment by bivariate methods at large scales: application to a complex mountainous environment. Geomorphology 92, 38–59.

Van Asch, T.W.J., Buma, J., Van Beek, L.P.H., 1999. A view on some hydrological triggering systems in landslides. Geomorphology 30, 25–32.

Van Asch, T.W.J., Malet, J.P., Van Beek, L.P.H., Amitrano, D., 2007. Techniques, issues and advances in numerical modelling of landslide hazard. Bulletin de la Société géologique de France 178, 65–88.

Van Den Eeckhaut, M., 2006. Spatial and temporal patterns of landslide in hilly regions. The Flemish Ardennes (Belgium). PhD Thesis, Katholieke Universiteit Leuven, Leuven, 250 pp.

Van Den Eeckhaut, M., Poesen, J., Verstraeten, G., Vanacker, V., Moeyersons, J., Nyssen, J., van Beek, L.P.H., 2005. The effectiveness of hillshade maps and expert knowledge in mapping old deep-seated landslides. Geomorphology 67, 351–363.

Van Den Eeckhaut, M., Vanwalleghem, T., Poesen, J., Govers, G., Verstraeten, G., Vandekerckhove, L., 2006. Prediction of landslide susceptibility using rare events logistic regression: a case-study in the Flemish Ardennes (Belgium). Geomorphology 76, 392–410.

Van Den Eeckhaut, M., Verstraeten, G., Poesen, J., 2007a. Morphology and internal structure of a dormant landslide in a hilly area: the Collinabos landslide (Belgium). Geomorphology 89, 258–273.

Van Den Eeckhaut, M., Poesen, J., Dewitte, O., Demoulin, A., De Bo, H., Vanmaercke-Gottigny, M.C., 2007b. Reactivation of old landslides: lessons learned from a case-study in the Flemish Ardennes (Belgium). Soil Use and Management 23, 200–211.

Van Den Eeckhaut, M., Reichenbach, P., Guzzetti, F., Rossi, M., Poesen, J., 2009. Combined landslide inventory and susceptibility assessment based on different mapping units: an example from the Flemish Ardennes, Belgium. Natural Hazards and Earth Systems Sciences 9, 507–521.

Van Westen, C.J., Rengers, N., Soeters, R., 2003. Use of geomorphological information in indirect landslide susceptibility assessment. Natural Hazards 30, 399–419.

Van Westen, C.J., Van Asch, T.W.J., Soeters, R., 2006. Landslide hazard and risk zonation — why is it still so difficult? Bulletin of Engineering Geology and the Environment 65, 167–184.

Van Westen, C.J., Castellanos, E., Kuriakose, S.L., 2008. Spatial data for landslide susceptibility, hazard, and vulnerability assessment; an overview. Engineering Geology 102, 112–131.

Yilmaz, I., 2009. Landslide susceptibility mapping using frequency ratio, logistic regression, artificial neural networks and their comparison: a case study from Katlandslides (Tokat—Turkey). Computers and Geosciences 35, 1125–1138.

Zimmermann, H.-J., 1991. Fuzzy Set Theory and Its Application. Kluwer Academic Publisher, Dordrecht. (399 pp.).